Applied Catalysis B: Environmental 119–120 (2012) 175–182

Contents lists available at SciVerse ScienceDirect

Applied Catalysis B: Environmental

journal homepage: www.elsevier.com/locate/apcatb

Nanostructured δ-FeOOH: An efficient Fenton-like catalyst for the oxidation of organics in water

Izabela S.X. Pinto[a], Pedro H.V.V. Pacheco[a], Jakelyne Viana Coelho[b], Eudes Lorençon[b], José D. Ardisson[c], José D. Fabris[d], Patterson P. de Souza[e], Klaus W.H. Krambrock[f], Luiz C.A. Oliveira[b,*], Márcio C. Pereira[a]

[a] Instituto de Ciência, Engenharia e Tecnologia, Universidade Federal dos Vales do Jequitinhonha e Mucuri, 39803-371 Teófilo Otoni, Minas Gerais, Brazil
[b] Departamento de Química, ICEx, Universidade Federal de Minas Gerais, 31270-901 Belo Horizonte, Minas Gerais, Brazil
[c] Centro de Desenvolvimento da Tecnologia Nuclear, 31270-901 Belo Horizonte, Minas Gerais, Brazil
[d] Universidade Federal dos Vales do Jequitinhonha e Mucuri, 39100-000 Diamantina, Minas Gerais, Brazil
[e] Departamento de Química, Centro Federal de Educação Tecnológica de Minas Gerais, 30480-000 Belo Horizonte, Minas Gerais, Brazil
[f] Departamento de Física, ICEx, Universidade Federal de Minas Gerais, 31270-901 Belo Horizonte, Minas Gerais, Brazil

ARTICLE INFO

Article history:
Received 21 October 2011
Received in revised form 6 February 2012
Accepted 23 February 2012
Available online 3 March 2012

Keywords:
Iron oxyhydroxide
Catalysis
Oxidation
Dyes
Fenton

ABSTRACT

δ-FeOOH nanoparticles were prepared by the precipitation of $Fe(OH)_2$ followed by rapid oxidation with H_2O_2. Samples with different surface areas and particle sizes were obtained by controlling the final pH of the reaction medium. The samples were characterized by X-ray powder diffractometry, ^{57}Fe Mössbauer spectroscopy, saturation magnetization measurements, total Fe chemical analyses and BET surface area measurements. The catalytic activities of these samples for H_2O_2 decomposition were strongly influenced by the δ-FeOOH surface area. EPR was used to monitor catalytic H_2O_2 decomposition in the presence of methanol, indicating that the mechanism of decomposition involves radicals in accord with the Haber–Weiss mechanism. Methylene blue and indigo carmine were used to simulate the degradation of contaminants. Monitoring these experiments with ESI-MS revealed that δ-FeOOH can activate H_2O_2 to produce reactive radicals, which can further promote the oxidation of the dyes. The dye degradation rates depended on the amount of Fe^{2+} generated *in situ* on the δ-FeOOH surface.

1. Introduction

In the last decade, several systems based on Fe-bearing solids, such as iron oxides [1–11], zeolites [12], pillared clays [13], and alumina [14], have been investigated for use in environmental remediation processes. Iron oxides are good candidates for use as heterogeneous Fenton-like catalyst because they are reactive at neutral pH. This avoids the need for the acidification and neutralization steps used in the homogeneous Fenton process and thereby avoids sludge formation. The heterogeneous catalysts can also be easily recycled, and all operations in the effluent treatment are significantly simplified if the solid catalyst is easy to handle.

Among the iron oxides, magnetite (ideal formula Fe_3O_4) has been widely reported as a suitable Fenton-like catalysis because of its magnetic and redox properties, which are strongly affected by the isomorphic substitution of Fe by others cations. For instance, the isomorphic substitution of Fe^{2+} by Co^{2+} or Mn^{2+} causes a significant increase in the reactivity of the system, whereas Ni^{2+} doping retards the catalytic activity of magnetite to activate the H_2O_2 molecule [3]. However, the main problem in the use of magnetite as a Fenton-like catalyst lies in is the atmospheric oxidation of structural Fe^{2+} to Fe^{3+}. This oxidation produces an outer Fe^{3+} oxide layer which passivates the magnetite surface and inhibits the catalytic efficiency toward Fenton-like catalysis.

Lee et al. [15] compared the catalytic efficiency of homogeneous Fenton and commercial goethite, hematite and magnetite to oxidize phenol in the presence of H_2O_2. The efficiency of the catalysts decreased in the sequence $Fe^{2+} \gg$ magnetite ≈ hematite > goethite. Composites based on goethite supported on a silica matrix to degrade phenol in the presence of H_2O_2 and oxalic acid. However, the reactivity of this system to oxidize phenol was correlated with dissolutive capacity of Fe by oxalic acid, and therefore homogeneous Fenton take place [16].

The use of iron oxides such as magnetite (Fe_3O_4) [1–3], hematite (α-Fe_2O_3) [4,5], maghemite (γ-Fe_2O_3) [6,7] and goethite (α-FeOOH) [6–9] as heterogeneous Fenton-like catalysts is very well documented in the literature. However, to the best of our knowledge, only one study [17] has reported the use of δ-FeOOH as a Fenton-like catalyst. No studies on the effects of the physical and chemical properties of δ-FeOOH on the catalytic properties have been reported.

* Corresponding author. Tel.: +55 31 3409 6384; fax: +55 31 34095700.
E-mail address: luizoliveira@qui.ufmg.br (L.C.A. Oliveira).

0926-3373/$ – see front matter © 2012 Elsevier B.V. All rights reserved.
doi:10.1016/j.apcatb.2012.02.026

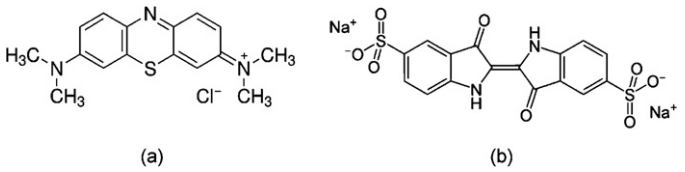

Fig. 1. Molecular structure of (a) methylene blue and (b) indigo carmine.

δ-FeOOH is a polymorph of four known iron oxyhydroxides, with a structure that is based on a hexagonal closed-packed oxygen lattice similar to that of hematite (α-Fe_2O_3) [18], where iron occupies half of the available octahedral interstices [19]. It presents some advantages for use in heterogeneous catalysis because (i) nanoparticles can be easily synthesized; (ii) the high surface area results in more contact between the catalyst, the H_2O_2 and the contaminant, thus increasing the efficiency of H_2O_2 activation and thereby the oxidation of organic compounds; (iii) it is ferrimagnetic at room temperature, thus the catalyst can be easily recovered after the reaction using a simple magnet and (iv) its synthesis is cheap due to the ample availability of the raw material, as iron is one of the most abundant elements on Earth.

Thus, the objective of the present study was to investigate the influence of the chemical and physical properties of δ-FeOOH nanoparticles on H_2O_2 decomposition and dye oxidation. δ-FeOOH materials with different particle sizes and surface areas were synthesized by the precipitation of $Fe(OH)_2$ followed by rapid oxidation with H_2O_2. The material's viability as a heterogeneous catalyst was tested by its ability to degrade a cationic dye (methylene blue) (Fig. 1a) and an anionic dye (indigo carmine) (Fig. 1b) in aqueous media.

2. Experimental methods

2.1. Synthesis of δ-FeOOH

The synthesis of δ-FeOOH was carried out using analytically pure chemicals and doubly distilled water. Because of strong foaming in the course of Fe^{2+} oxidation with H_2O_2, the sample was prepared in a specially designed glass reactor. In short, 200 mL of a solution containing 5.5604 g of $FeSO_4(NH_4)_2SO_4{\cdot}6H_2O$ was mixed with 200 mL of a 2 M NaOH solution. A green precipitate (green rust) was formed. Immediately, 5 mL of 30% H_2O_2 was added with stirring. The precipitate turned reddish brown within a few seconds, indicating the formation of δ-FeOOH. δ-FeOOH samples with different particle sizes and surface areas were obtained by changing the final pH of the suspension by adding concentrated HCl or NaOH solutions and monitoring the pH with test strips. The precipitate was washed with distilled water several times and dried in a vacuum desiccator at room temperature. The samples were labeled according to the final pH of the suspension, *i.e.*, F12, F12.5, F13.5 and F14.

2.2. Characterization

The total Fe content of the δ-FeOOH samples was determined by volumetric titration with a $K_2Cr_2O_7$ solution. Saturation magnetization measurements were performed using a portable magnetometer [20]. Surface areas were determined by the BET method using a 22 point N_2 adsorption/desorption procedure in an Autosorb 1 Quantachrome gas sorption analyzer.

X-ray diffraction (XRD) was carried out using Cu-Kα radiation with a Rigaku Geigerflex diffractometer equipped with a graphite diffracted-beam monochromator. Data were collected from 20° to 70° 2θ in steps of 0.02° per 5-s iteration.

Mössbauer spectra were collected in constant acceleration transmission mode with a 10 mCi ^{57}Co/Rh source. The spectra of δ-FeOOH samples were taken at 298 K and at 20 K using a liquid helium bath cryostat. Doppler velocities ranged between ± 2 mm s^{-1} at room temperature and ± 12 mm s^{-1} at 20 K. The data were stored in a 1024-channel MCS memory unit and were fitted using the NORMOS program. Isomer shifts were calculated relative to α-Fe.

2.3. Catalytic tests

Hydrogen peroxide (2.8 M) decomposition was studied by measuring the formation of gaseous O_2 in a volumetric glass system at pH ≈ 6.3 using 30 mg catalyst aliquots.

The oxidation of 0.04 g L^{-1} methylene blue with H_2O_2 was carried out at pH 6 in the presence of 30 mg of catalyst and monitored by UV/vis spectroscopy at 663 nm, using a Varian Cary 5 spectrometer.

The oxidation of 0.05 g L^{-1} indigo carmine with H_2O_2 was carried out at pH 6.5 in the presence of 30 mg of catalyst and monitored by UV/vis spectroscopy at 612 nm using a Varian Cary 5 spectrometer. All reactions were performed at 26 ± 1 °C in a recirculating temperature-controlled bath. The Fe concentrations in the solutions after the reactions were determined by atomic absorption spectrometry using a Varian SpectrAA210 spectrometer.

2.4. Electrospray ionization (ESI)-mass spectrometry (MS)

To identify the intermediate chemical species of the methylene blue oxidation reaction, an ION-TRAP LCQFleet (ThermoScientific, San Jose, CA) was used in positive ion mode. The reaction samples were analyzed by introducing aliquots into the ESI source with a syringe pump at a flow rate of 15 L min^{-1}. Spectra were obtained as averages of 5 scans of 0.2 s each. Typical ESI conditions used a heated capillary temperature of 275 °C, sheath gas (N_2) at a flow rate of 15 units (ca. 4 L min^{-1}), a spray voltage of 2 kV, a capillary voltage of 25 V and a tube lens offset voltage of 25 V.

2.5. EPR study

To investigate the possibility of the formation of radical species in our system, an EPR study was performed. In a typical experiment, 10 mg of a δ-FeOOH sample were dispersed into 10 mL of a 2 wt.% poly(vinyl alcohol) aqueous solution. The reaction was initiated by the addition of 10 mL of cyclohexane containing 10 mM of PBN (N-t-Butyl-α-phenylnitrone) and 0.1 mL of hydrogen peroxide (30% v/v) to the emulsion with vigorous stirring. Then, 100 μL aliquots from the cyclohexane organic phase (the upper layer) were quickly transferred to a precision bore quartz EPR tube with a diameter of 3 mm. The (EPR) spectra were recorded at room temperature with a custom-built X-band spectrometer (9.38 GHz) using a commercial cylindrical cavity (Bruker), a klystron (Varian) and an electromagnet (Varian) with a maximum field amplitude of 800 mT. For the *g* factor calibration, 1,1-diphenyl-2-picrylhydrazyl (DPPH) was used as the standard ($g = 2.0037$).

3. Results and discussion

3.1. Characterization of the δ-FeOOH samples

The δ-FeOOH samples were prepared by the precipitation of $Fe(OH)_2$ followed by rapid oxidation with H_2O_2. The XRD patterns of samples F14, F13.5 and F12.5 (Fig. 2) showed a single phase corresponding to δ-FeOOH, which was identified by 1 0 0, 1 0 1, 1 0 2 and 1 1 0 diffraction maxima consistent with those of JCPDS File

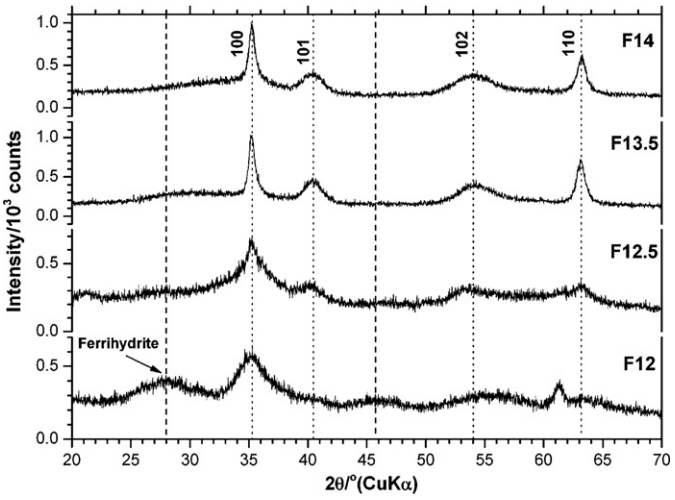

Fig. 2. X-ray powder diffraction patterns of the δ-FeOOH samples.

No. 13-87. In addition to the δ-FeOOH, the XRD pattern of sample F12 revealed the presence of 2-line ferrihydrite ($Fe_5HO_8{\cdot}4H_2O$), which was identified by its reflections at approximately 28° and 46° in 2θ. The δ-FeOOH became less crystalline as the final pH of the synthesis decreased, which was verified by the broadening of the diffraction peaks (Fig. 2). The 1 1 0 reflection in sample F12 was shifted to lower angles with respect to the other samples, but no explanation for this can be given based on the currently available data. The pronounced differential line broadening of the 1 0 0, 1 0 1, 1 0 2 and 1 1 0 reflections indicates anisotropic crystal growth. The mean crystallite dimension for samples F14, F13.5, F12.5 and F12 estimated from the 1 0 0 reflection using the Scherrer equation are shown in Table 1. The particle size decreased as the final pH of synthesis decreased.

The room-temperature Mössbauer spectra (Fig. 3) did not show magnetic ordering due to the superparamagnetic behavior of the synthetic nanoparticles. The slight asymmetry observed in the spectra indicates that the iron may be distributed in different sites in the δ-FeOOH structure.

To better understand the distribution of iron in the δ-FeOOH structure, Mössbauer spectra were also collected at 20 K. The spectra of all samples (Fig. 4a) were fitted with a magnetic hyperfine field (B_{hf}) distribution for B-site of δ-FeOOH (Fig. 4b) due to the particle size distribution. The two main magnetically split components correspond to iron in octahedral sites in the δ-FeOOH structure. In addition to these two magnetically split components, the spectrum of sample F12 exhibited a paramagnetic contribution due to the presence of ferrihydrite, as verified by XRD. The Mössbauer parameters (Table 2) revealed a markedly lower hyperfine field than that of bulk δ-FeOOH (50.8 T for site A and 53 T for site B [21]), due to superparamagnetic relaxation effects. Superparamagnetic relaxation can be described by Eq. (1):

$$\tau = \tau_0 e^{(KV/kT)} \quad (1)$$

Table 1
Fe content, saturation magnetization and mean crystallite dimension of the δ-FeOOH samples.

Sample	Fe content (wt.%)	σ (J T^{-1} kg^{-1})	MCD (nm)
F14	62.0(3)	7.10(3)	15
F13.5	55.3(1)	5.26(5)	14
F12.5	49.2(4)	0.04(2)	6
F12	32.2(3)	0.03(1)	2

σ = saturation magnetization, MCD = mean crystallite dimension.

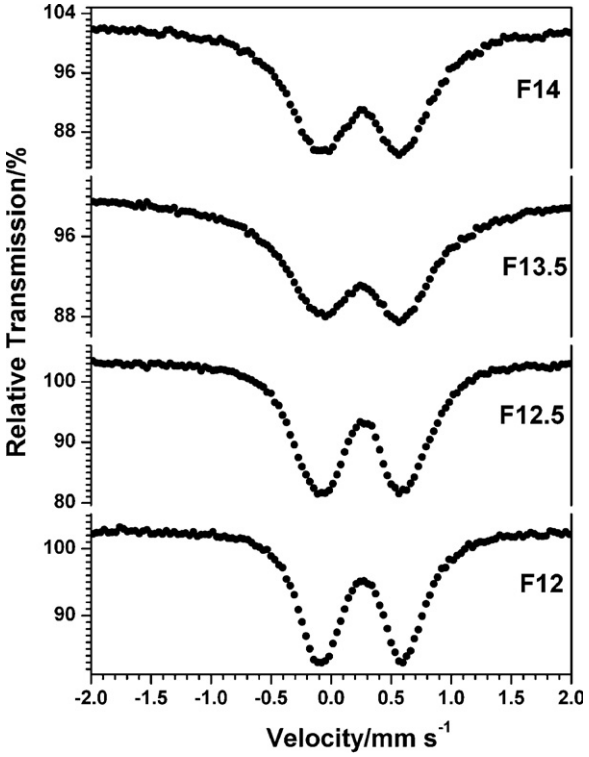

Fig. 3. 298 K Mössbauer spectra of the δ-FeOOH samples.

where τ is the relaxation time, τ_0 is a constant in the order of 10^{-10} s, K is the anisotropy constant (a measure of the resistance of the particle to spin direction reversals), V is the particle volume, k is the Boltzmann constant and T is the temperature. If the spin reversals occur more rapidly than the nucleus can follow ($\tau_L \approx 10^{-8}$ s for ^{57}Fe), the result will be a net reduction of the hyperfine field, which can approach zero for sufficiently small particles. Thus, the reduction in the hyperfine field can be expressed by Eq. (2):

$$B_{hf}(V,T) = B_{hf}(V=\infty,T)\langle\cos\theta\rangle \quad (2)$$

in which $B_{hf}(V=\infty, T)$ is the hyperfine field in a large crystal at the same temperature and θ is the angle between the direction of the magnetic moment and the easy direction of magnetization. Thus, the decrease in the hyperfine field with respect to bulk δ-FeOOH could be indicative of the small particle size of the materials indicated by XRD.

Table 2
Hyperfine parameters obtained from fit of the Mössbauer spectra of the δ-FeOOH samples.

Sample	δ (mm s^{-1})	$\Delta, 2\varepsilon$ (mm s^{-1})	B_{hf} (T)	W (mm s^{-1})	RA (%)	Fe site
F14	0.49	−0.08	47.5	0.31[a]	56.5	Ft-A
	0.49	−0.07	51.3	0.57	43.5	Ft-B
F13.5	0.49	−0.15	44.7	0.31[a]	81.2	Ft-A
	0.48	−0.16	49.1	0.68	18.8	Ft-B
F12.5	0.48	−0.14	44.2	0.31[a]	77.1	Ft-A
	0.50	−0.17	49.1	0.86	22.9	Ft-B
F12	0.44	−0.25	42.4	0.31[a]	55.6	Ft-A
	0.51	−0.20	43.5	0.77	31.8	Ft-B
	0.53	0.96		0.71	12.6	Fh

δ = isomer shift relative to α-Fe; 2ε = quadrupole shift, Δ = quadrupole splitting; B_{hf} = magnetic hyperfine field; W = full width at half height; RA = relative subspectral area.

[a] Value fixed.

Ft = δ-FeOOH, Fh = ferrihydrite.

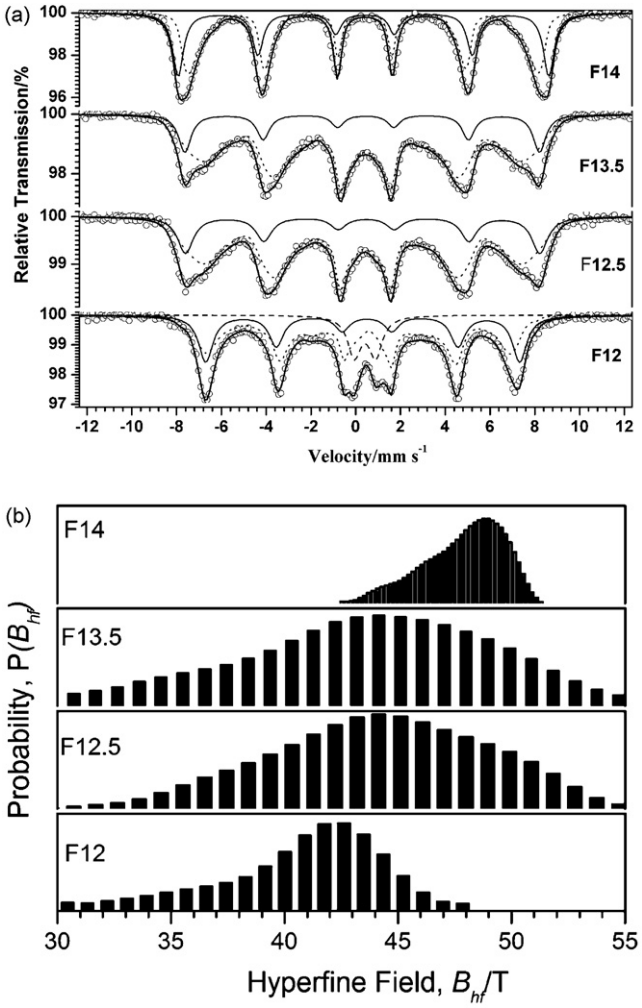

Fig. 4. (a) 20 K Mössbauer spectra of the δ-FeOOH samples. (b) Hyperfine field distribution for B-site of δ-FeOOH.

The isomer shifts of 0.49–0.51 mm s^{-1} show that Fe^{3+} is located only on octahedrally coordinated sites. The two components observed by Mössbauer spectroscopy can be interpreted on the basis of the structural model proposed by Chukhrov et al. [22], in which the Fe atoms on site B are located according to the hematite pattern (two occupied octahedral units regularly alternating with a vacant octahedron along [1 1 0]: Fe–Fe–⊗–Fe. . .), and the Fe atoms on site A are distributed according to an anti-hematite pattern (two vacant octahedral units alternating with an occupied octahedron: ⊗–⊗–Fe–⊗. . .).

The iron content of all samples (Table 1) was lower than expected from the ideal formula (62.9 wt.%), which suggests the presence of surplus water adsorbed on the surface, in the pores and possibly also within the structure of δ-FeOOH. The iron content in the δ-FeOOH samples decreased with the final pH of synthesis.

The saturation magnetization (σ) values of the samples at room temperature (Table 1) was lower than that of bulk δ-FeOOH (20 J T^{-1} kg^{-1}) [21]. The decrease in the magnetization value is due to the small particle size and the lower iron content observed for these samples compared with bulk δ-FeOOH. It was observed that the magnetization values decreased as the final pH of synthesis decreased. Samples F12.5 and F12 did not exhibit noticeable spontaneous magnetization at room temperature.

The N_2 adsorption–desorption isotherms for the δ-FeOOH samples obtained at different pHs are shown in Fig. 5. The isotherm of sample F13.5 exhibited high N_2 adsorption and reached

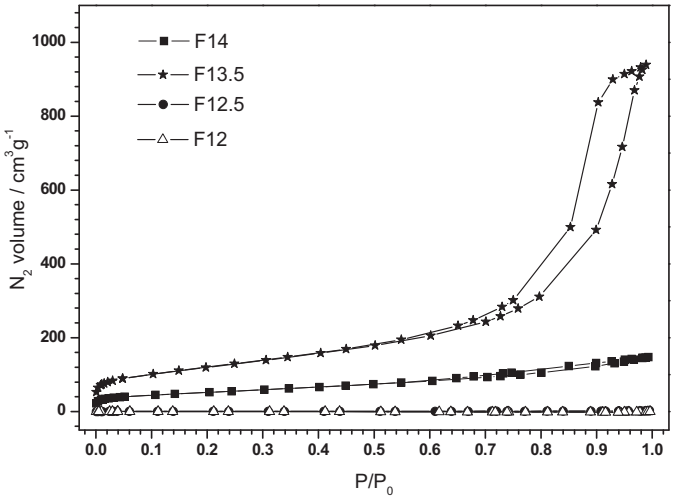

Fig. 5. N_2 adsorption–desorption isotherms of the δ-FeOOH samples.

914 cm^3 g^{-1} at $p/p_0 = 0.95$, which is an indicative of a material with an extremely high pore volume. The F13.5 sample exhibited a type IV isotherm, characteristic of mesoporous materials and a type H1 hysteresis loop, which is related to the filling of the mesopores due to capillary condensation. In addition, this material had a high surface area (419 m^2 g^{-1}). A large distribution of porous volumes was observed in the materials due to the different pH values in the syntheses of the δ-FeOOH samples. Sample F14 had a lower adsorption capacity for nitrogen compared with F13.5. Indeed, at $p/p_0 = 0.95$, it absorbed only 140 cm^3 g^{-1} of nitrogen. Moreover, F14 presented a type IV isotherm with a small type H4 hysteresis loop and a BET surface area of 183 m^2 g^{-1}. A significant reduction in the volume of adsorbed nitrogen was also observed when the synthesis was performed at lower pH values. All materials produced below pH 13 exhibited poor nitrogen adsorption capacities, as can be seen in the low surface areas found for samples F12 and F12.5.

3.2. H_2O_2 decomposition

The δ-FeOOH samples were used to catalyze hydrogen peroxide decomposition (Eq. (3)). H_2O_2 decomposition is a versatile reaction for probing the activity of heterogeneous systems in Fenton-like processes.

$$2H_2O_2 \xrightarrow{\delta FeOOH} 2H_2O + O_2 \quad (3)$$

The results of H_2O_2 decomposition in the presence of the δ-FeOOH samples are shown in Fig. 6. Samples F14 and F13.5 promoted H_2O_2 decomposition more efficiently than the other samples. The superior catalytic activity of samples F14 and F13.5 may be attributed to their high surface area and mesoporous structures, which allow better accessibility of H_2O_2 to the inner surfaces of these materials.

The approximately linear behavior of the decomposition plots suggests that the reaction has a pseudo zeroth order dependence on the H_2O_2 concentration. The reaction rates could then be estimated by linear fits of the decomposition plots. The obtained rate constants for H_2O_2 decomposition were 13.4(2) mM min^{-1} for F12, 5.4(1) mM min^{-1} for F12.5, 20.0(2) mM min^{-1} for F13.5 and 11.2(2) mM min^{-1} for F14.

To evaluate whether the H_2O_2 decomposition mediated by δ-FeOOH takes place *via* a radical mechanism, H_2O_2 decomposition measurements were carried out with sample F13.5 in the presence of methanol, which is known be a hydroxyl radical scavenger [23].

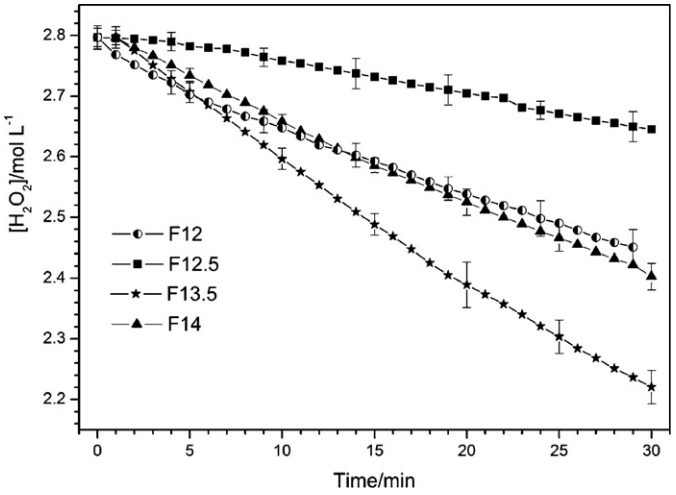

Fig. 6. H_2O_2 decomposition in the presence of the δ-FeOOH samples. Catalyst = 30 mg, $[H_2O_2]$ = 2.8 M, pH 6.2, temperature = 26 °C.

Fig. 7 shows the H_2O_2 decomposition kinetics in the presence of different concentrations of methanol. The H_2O_2 decomposition was strongly inhibited in the presence of methanol. The pseudo zeroth order rate constants obtained were 20.0(2) mM min^{-1} for 0% methanol, 4.8(1) mM min^{-1} for 25% methanol, 3.9(1) mM min^{-1} for 35% methanol, 2.9(3) mM min^{-1} for 50% methanol and 1.2(1) mM min^{-1}.

The inhibition of the H_2O_2 decomposition reaction could be due to a competitive process involving methanol and the active Fe surface that could be related to (i) the adsorption of methanol on the active sites of δ-FeOOH and/or (ii) the reaction of methanol with intermediate species of H_2O_2 decomposition such as $^{\bullet}OH$ and $O_2^{\bullet-}$ radicals.

3.3. Dye discoloration studies

The dye discoloration studies were carried out using two different dyes: (i) a cationic dye, *i.e.*, methylene blue (Fig. 1a) and (ii) an anionic dye, *i.e.*, indigo carmine (Fig. 1b). These dyes are suitable for probing molecular oxidation reactions because (i) they show high solubility in water, (ii) the discoloration reactions can be monitored by simple spectrophotometric measurements and (iii) they simulate the behavior of textile dyes, which are an important class of contaminant [24,25].

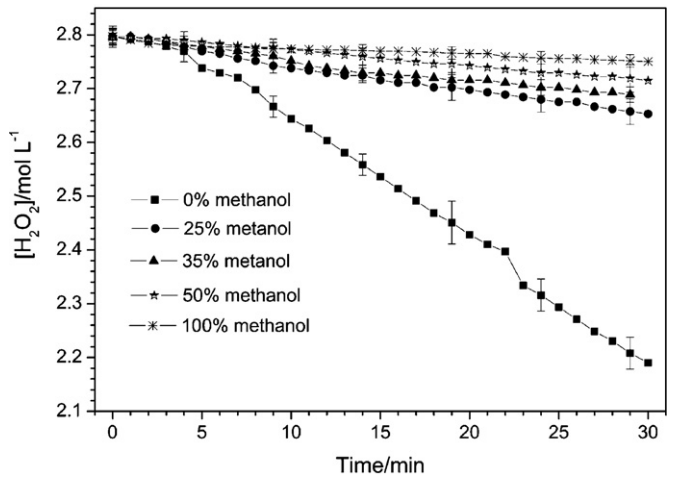

Fig. 7. H_2O_2 decomposition in the presence of sample F13.5 and different concentrations of methanol. Catalyst = 30 mg, $[H_2O_2]$ = 2.8 M, pH 6.2, temperature = 26 °C.

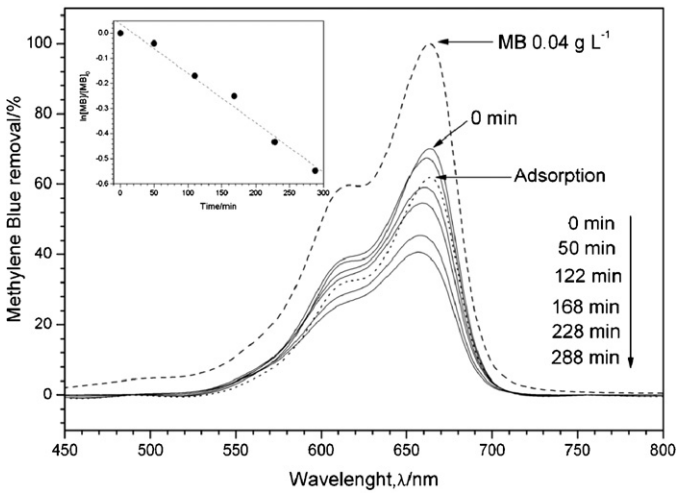

Fig. 8. Methylene blue (MB) discoloration in the presence of sample F13.5 and H_2O_2. Catalyst weight = 30 mg, $[MB]_{initial}$ = 0.04 g L^{-1}, $[H_2O_2]$ = 0.25 M, $pH_{initial}$ 6. Inset: ln $[MB]/[MB]_0$ vs. time.

Dye discoloration is attributed to two main processes: (i) adsorption on the δ-FeOOH surface and (ii) dye oxidation to produce non-colored species. Figs. 8 and 9 indicate that the indigo carmine exhibits greater adsorption on the δ-FeOOH surface (sample F13.5) than the methylene blue. The adsorption capacities of MB or IC per gram of δ-FeOOH at 26 °C were estimated to be 5.1 mg g^{-1} and 11.6 mg g^{-1}, respectively. A simple electrostatic interaction model can explain this difference. The pH used in the adsorption experiments was below the point of zero charge of δ-FeOOH (pzc = 8.5) [17], and if the δ-FeOOH surface is positively charged, *i.e.*, the anionic dyes are more easily attracted to the δ-FeOOH surface than the cationic dyes.

The oxidation of methylene blue and indigo carmine with H_2O_2 in the presence of δ-FeOOH (sample F13.5) was spectrophotometrically monitored (Figs. 8 and 9). After the addition of H_2O_2, a portion of the adsorbed methylene blue and indigo carmine was desorbed from the δ-FeOOH surface. This suggests a competitive adsorption pathway between H_2O_2 and the dyes. The gradual discoloration of dyes over time was also observed after the addition of H_2O_2, which suggests that the Fe^{3+} species on the δ-FeOOH surface can initiate

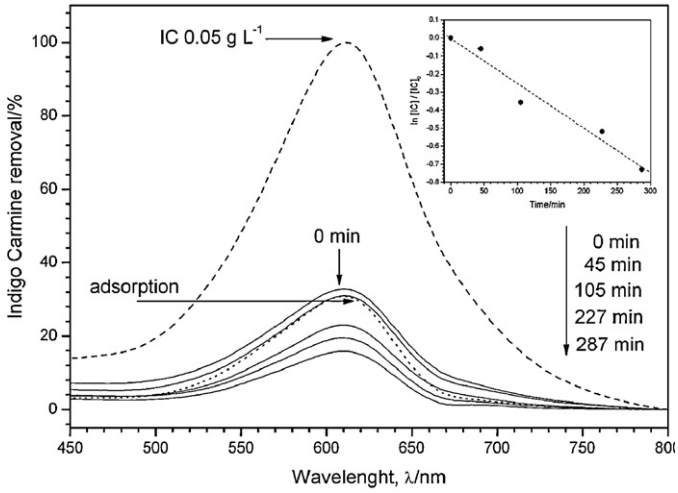

Fig. 9. Indigo carmine (IC) discoloration in the presence of sample F13.5 and H_2O_2. Catalyst weight = 30 mg, $[IC]_{initial}$ = 0.05 g L^{-1}, $[H_2O_2]$ = 0.25 M, $pH_{initial}$ 6. Inset: ln $[IC]/[IC]_0$ vs. time.

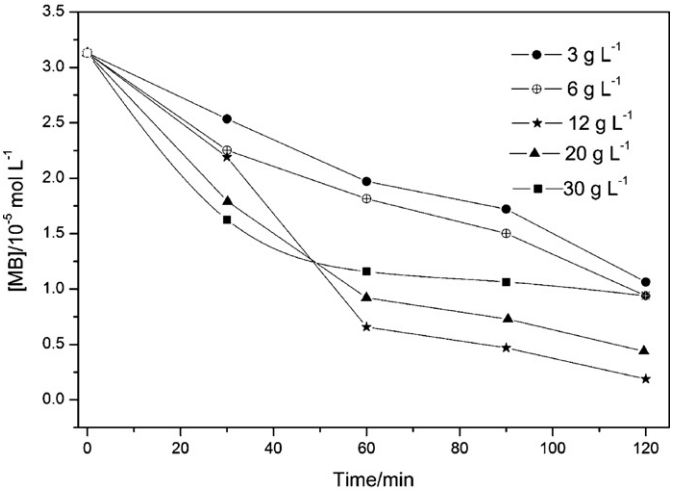

Fig. 10. Methylene blue (MB) discoloration in the presence of sample F13.5 and different H_2O_2 concentration. Catalyst weight = 30 mg, $[MB]_{initial}$ = 0.01 g L^{-1}, $pH_{initial}$ 6.

the H_2O_2 activation by generating reactive radicals such as •OH and $O_2^{\bullet -}$, which are able to oxidize the organic dyes.

Although the kinetics in these reactions are very complex, the data could be fitted to a first order dependence on the dye concentrations (Figs. 8 and 9, inset). This could be due to the relatively high initial concentration of H_2O_2 and the active sites of the catalyst, which do not change significantly at the beginning of the reaction. The pseudo first order rate constants estimated for the oxidation of the methylene blue and indigo carmine dyes were $1.59(1) \times 10^{-4}$ min^{-1} m^{-2} and $1.99(2) \times 10^{-4}$ min^{-1} m^{-2}, respectively.

The effect of H_2O_2 on the degradation rates of MB was evaluated and the results are shown in Fig. 10. At high H_2O_2 concentrations (above 12 g L^{-1}), the degradation rate of MB was decreased (Fig. 11) because H_2O_2 acts as a scavenger for hydroxyl radicals. The optimal H_2O_2 concentration for MB oxidation was 12 g L^{-1}.

Atomic absorption analysis of the supernatant after the reactions did not show a significant concentration of soluble iron (<0.08 μg L^{-1}). Moreover, no significant change in the color of dyes was observed after the removal of the catalyst from the reaction medium by a simple magnetic separation, which suggests that the mechanism of the dye degradation is in fact based on a heterogeneous reaction initiated at the δ-FeOOH surface.

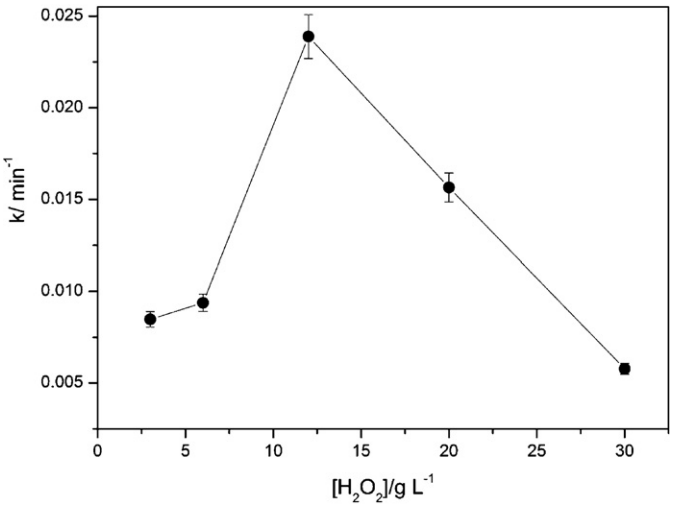

Fig. 11. Rate constant vs. H_2O_2 concentration.

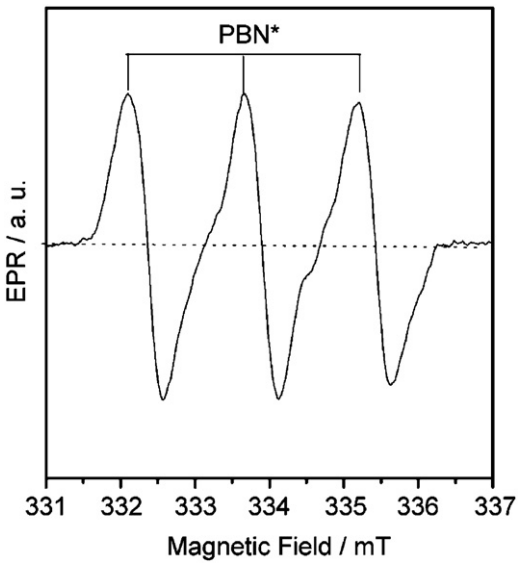

Fig. 12. EPR spectrum of PBN spin-adduct in cyclohexane for δ-FeOOH/H_2O_2 system.

3.4. Reaction mechanism

The results obtained in this work suggest that δ-FeOOH has a strong effect on the reactivity for H_2O_2 decomposition and can promote the oxidation of both methylene blue and indigo carmine dyes.

The results from H_2O_2 decomposition in the presence of the catalyst and methanol (Fig. 7) support the presence of radicals in the reaction system. The rate constant of H_2O_2 decomposition decreased when the methanol concentration increased. This inhibition of H_2O_2 decomposition could be attributed to methanol acting as a hydroxyl radical trap, thereby decreasing O_2 evolution.

The radical specimens produced by the δFeOOH/H_2O_2 system were investigated by EPR spectroscopy. Fig. 12 shows the EPR spectrum of a cyclohexane solution after δFeOOH was treated with H_2O_2. The spectrum is characterized by PBN (N-t-Butyl-α-phenylnitrone) spin-adducts with $g = 2.0060(1)$ and a nitrogen hyperfine interaction from the nitrone group of PBN of $a^N = 15.4(1)$ G. No additional proton hyperfine interaction was observed, probably due to the large linewidth of $\Delta B_{pp} = 4.0(2)$ G. Control experiments performed in the absence of δFeOOH or H_2O_2 did not show EPR signals. These results are consistent with the formation of •OH PBN spin-adducts [26], confirming that the mechanism of organic oxidation in the presence of δFeOOH and H_2O_2 occurs *via* free radicals.

ESI-MS experiments using MB and the δFeOOH/H_2O_2 system (Fig. 13) showed a strong signal at $m/z = 391$, probably due to successive hydroxylation of the MB aromatic ring. This strongly suggests that the reaction with this catalyst is initiated by the activation of H_2O_2 in the presence of δFeOOH to produce •OH radicals, as verified by EPR. Moreover, at zero reaction time, the ESI-MS operating in positive mode showed the presence of only a single cation ($m/z = 284$) in aqueous solution (Fig. 13a). After 60 min of reaction, the intense peak at $m/z = 284$ decreased, and new peaks with $m/z = 129$, 149, 260 and a more intense peak at $m/z = 391$ emerged (Fig. 13b). The MS/MS spectrum of the peak with $m/z = 391$ (Fig. 14) indicates the rupture of the MB ring to produce a new molecule with $m/z = 149$. The rupture of the MB aromatic ring is due to successive hydroxylation promoted by •OH radicals [25]. The ion $m/z = 149$ appears as a result of the degradation of MB and as the fragmentation product ion of $m/z = 391$ (Figs. 13b and c and 14). Thus, it is possible to associate the presence of the ion of $m/z = 391$ as a reaction of the ion $m/z = 149$ with another molecule

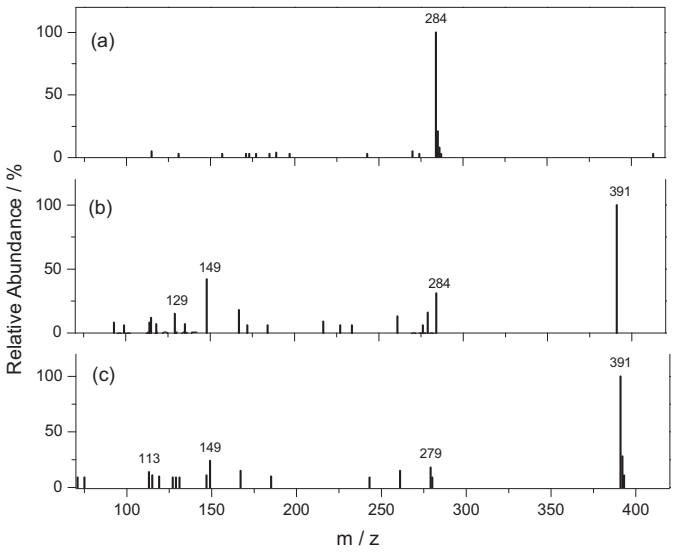

Fig. 13. ESI-(+)-MS of (a) standard methylene blue, (b) after 60 min reaction with δFeOOH/H_2O_2 and (c) after 300 min reaction with δFeOOH/H_2O_2.

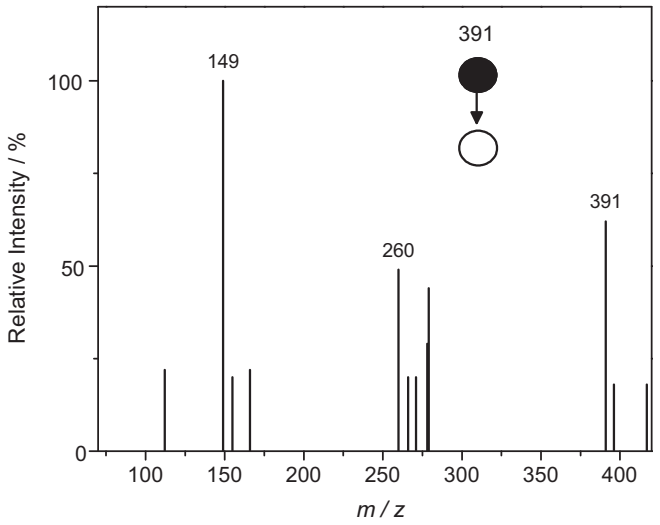

Fig. 14. ESI-(+)-MS/MS for the ion 391 (25 eV).

(m/z = 260) derived from successive oxidation of methylene blue [25], as shown in the spectrum fragmentation of ion m/z = 391 (Fig. 14). Proposals of these intermediates are shown in Fig. 15. A proposed structure of the ion m/z = 391 is shown in Fig. 16. Based on the fragmentation spectrum of this ion (Fig. 14), it was proposed a reaction between deprotonated molecules with MM = 148 g mol^{-1} and MM = 259 g mol^{-1} (Fig. 15). This reaction occurs with release of ammonia and subsequent protonation of the product.

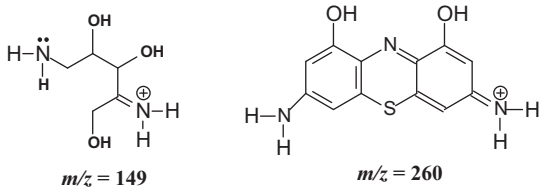

Fig. 15. Proposal of the reaction intermediates of MB oxidation with δFeOOH/H_2O_2.

After 300 min (Fig. 13c), the m/z = 284 peak disappeared completely and hydroxylated intermediates were observed. The relative intensity of the peak with m/z = 149 with respect to the peak with m/z = 391 decreased in comparison with the spectrum after 60 min, suggesting that the successive hydroxylation of MB molecule can lead to its complete mineralization.

Thus, although dye degradation occurs through several parallel reactions, we suggest a simplified pathway to describe the reaction. In this mechanism, the •OH radicals are produced through a reaction between H_2O_2 and δFeOOH. The •OH acts as the reactive species and oxidizes MB. Hence, a possible mechanism for MB degradation may be represented by four steps:

Step one: H_2O_2 adsorbs on the δ-FeOOH surface.

$$Fe_{surface}{}^{3+} + H_2O_{2(aq)} \rightarrow [Fe_{surface}{}^{3+}H_2O_{2(adsorbed)}] \quad (4)$$

Step two: adsorbed H_2O_2 reacts with active sites on the δ-FeOOH structure to form surface Fe^{2+} and $O_2^{\bullet -}$ radicals [1].

$$[Fe_{surface}{}^{3+}H_2O_{2(adsorbed)}] \rightarrow Fe_{surface}{}^{2+} + O_2^{\bullet -} + 2H^+ \quad (5)$$

Step three: the adsorbed H_2O_2 reacts with Fe^{2+} generated *in situ* to form highly active •OH radicals.

$$Fe_{surface}{}^{2+}H_2O_{2(adsorbed)} \rightarrow Fe_{surface}{}^{3+} + {}^{\bullet}OH + {}^{-}OH \quad (6)$$

Step four: the •OH radical attacks the dyes molecules to produce oxidized products.

$$^{\bullet}OH + \text{dyes} \rightarrow \text{oxidation products} \quad (7)$$

Thus, the dye degradation rate depends on the •OH formation rate, which in turn depends on the sum of active sites. The dye degradation rate equation can therefore be expressed as:

$$V_{Dye} = k[Dye][^{\bullet}OH] = k[Dye] \rightarrow [Fe_{surface}{}^{2+}H_2O_{2(adsorbed)}] \quad (8)$$

At equilibrium, the H_2O_2 adsorption on the δ-FeOOH can be written according to the Langmuir model. A similar model has been described by Lin and Gurol [27].

$$[Fe_{surface}{}^{2+}H_2O_{2(adsorbed)}] = [Fe_{surface}{}^{2+}]_{total}\frac{K_{ads}[H_2O_2]}{1 + K_{ads}[H_2O_2]} \quad (9)$$

The adsorption rate is given by

$$K_{ads} = \frac{[Fe_{surface}{}^{2+}H_2O_{2(adsorbed)}]}{[Fe_{surface}{}^{2+}][H_2O_2]} \quad (10)$$

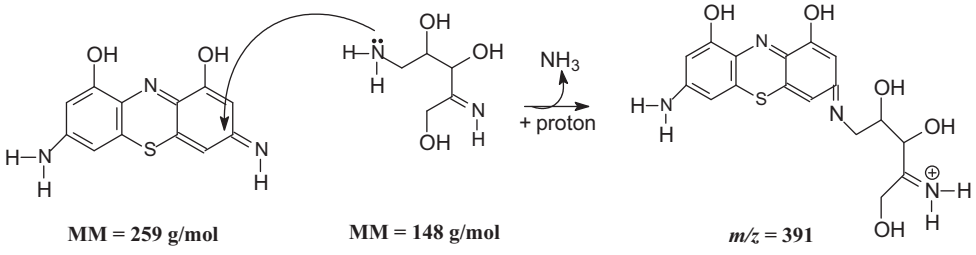

Fig. 16. Proposed structure for the ion m/z = 391.

The concentration of Fe^{2+} sites (free and occupied) is defined by:

$$[Fe_{surface}{}^{2+}]_{total} = [Fe_{surface}{}^{2+}H_2O_{2(adsorbed)}] + [Fe_{surface}{}^{2+}] \quad (11)$$

Substituting Eq. (9) in Eq. (8) gives the dye degradation rate equation (Eq. (12)):

$$V_{Dye} = k[Dye][^{\bullet}OH] = k\,[Dye]\,[Fe_{surface}{}^{2+}]_{total}\,\frac{K_{ads}[H_2O_2]}{1 + K_{ads}[H_2O_2]} \quad (12)$$

By this mechanism, the [•OH] depends on the concentration of Fe^{2+} generated *in situ* on the δ-FeOOH surface. Thus, the rate constant for dye degradation is pseudo first order in [Dye] and first order in [catalyst]. With respect to $[H_2O_2]$, two different reaction orders can be observed: (i) at low concentrations, the reaction is first order in $[H_2O_2]$ and (ii) at high concentrations, the reaction is zeroth order in $[H_2O_2]$.

4. Conclusions

The present work has shown that δ-FeOOH nanoparticles with different surface areas and porous structures can be synthesized by a simple method. The H_2O_2 decomposition catalyzed by these particles takes place *via* a radical mechanism, initiated by Fe^{3+} on the δ-FeOOH structure. The large surface area and mesoporous structure presented by samples F14 and F13.5 have an important role in the adsorption of both H_2O_2 and dyes on the δ-FeOOH surface. The adsorption of anionic dyes on the δ-FeOOH is favored over the adsorption of cationic dyes. The oxidation of dyes such as methylene blue and indigo carmine can be achieved with δ-FeOOH in the presence of H_2O_2. Experimental evidence clearly indicates that the degradation occurs on the catalyst surface and that the contributions of soluble Fe can be ignored. The •OH radicals may be the main species responsible for dye discoloration, and the •OH concentration depends strongly on the Fe^{2+} generated *in situ* at the δ-FeOOH surface.

Acknowledgment

The authors are grateful to FAPEMIG (APQ-04333-10), CAPES, CNPq and PRPq/UFMG for financial support.

References

[1] M.C. Pereira, L.C.D. Cavalcante, F. Magalhães, J.D. Fabris, J.W. Stucki, L.C.A. Oliveira, E. Murad, Chem. Eng. J. 166 (2011) 962–969.
[2] F. Magalhães, M.C. Pereira, S.E.C. Botrel, J.D. Fabris, W.A. Macedo, R. Mendonça, R.M. Lago, L.C.A. Oliveira, Appl. Catal. A-Gen. 332 (2007) 115–123.
[3] R.C.C. Costa, M.F.F. Lelis, L.C.A. Oliveira, J.D. Fabris, J.D. Ardisson, R.R.V.A. Rios, C.N. Silva, R.M. Lago, J. Hazard. Mater. B129 (2006) 171–178.
[4] L.C.A. Oliveira, F. Zaera, I. Lee, D.Q. Lima, T.C. Ramalho, A.C. Silva, E.M.B. Fonseca, Appl. Catal. A-Gen. 368 (2009) 17–21.
[5] A.L. Andrade, D.M. Souza, M.C. Pereira, J.D. Fabris, R.Z. Domingues, J. Nanosci. Nanotechnol. 9 (2009) 3695–3699.
[6] W.F. Souza, I.R. Guimarães, D.Q. Lima, C.L.T. Silva, L.C.A. Oliveira, Energy Fuel 23 (2009) 4426–4430.
[7] M.C. Pereira, F.S. Coelho, C.C. Nascentes, J.D. Fabris, M.H. Araújo, K. Sapag, L.C.A. Oliveira, R.M. Lago, Chemosphere 81 (2010) 7–12.
[8] L.C.A. Oliveira, M. Gonçalves, M.C. Guerreiro, T.C. Ramalho, J.D. Fabris, M.C. Pereira, K. Sapag, Appl. Catal. A-Gen. 316 (2007) 117–124.
[9] I. Guimarães, L.C.A. Oliveira, P.F. Queiroz, T.C. Ramalho, M.C. Pereira, J.D. Fabris, J.D. Ardisson, Appl. Catal. A-Gen. 347 (2008) 89–93.
[10] I.R. Guimarães, A. Giroto, L.C.A. Oliveira, M.C. Guerreiro, D.Q. Lima, J.D. Fabris, Appl. Catal. B-Environ. 91 (2009) 581–586.
[11] A.C. Silva, R.M. Cepera, M.C. Pereira, D.Q. Lima, J.D. Fabris, L.C.A. Oliveira, Appl. Catal. B-Environ. 107 (2011) 237–244.
[12] S.B.C. Pergher, L.C.A. Oliveira, A. Smaniotto, D.I. Petkowicz, Quim. Nova 28 (2005) 751–755.
[13] J.H. Ramirez, C.A. Costa, L.M. Madeira, G. Mata, M.A. Vicente, M.L. Rojas-Cervantes, A.J. López-Peinado, R.M. Martín-Aranda, Appl. Catal. B-Environ. 71 (2007) 44–56.
[14] M.S. Yalfani, S. Contreras, F. Medina, J. Sueiras, Appl. Catal. B-Environ. 89 (2009) 519–526.
[15] S. Lee, J. Oh, Y. Park, Bull. Korean Chem. Soc. 27 (2006) 489–494.
[16] C.P. Huang, Y.H. Huang, Appl. Catal. A-Gen. 346 (2008) 140–148.
[17] W. Du, Y. Xu, Y. Wang, Langmuir 24 (2008) 175–181.
[18] C.B. Koch, C.A. Oxborrow, S. Morup, M.B. Madsen, A.J. Quinn, J.M.D. Coey, Phys. Chem. Miner. 22 (1995) 333–341.
[19] G. Patrat, F. Bergevin, M. Pernet, J.C. Joubert, Acta Crystallogr. B39 (1983) 165–170.
[20] J.M.D. Coey, O. Cugat, J. McCauley, J.D. Fabris, Rev. Fis. Apl. Instrum. 7 (1992) 25–30.
[21] R.M. Cornell, U. Schwertmann, The Iron Oxides – Structure, Properties, Reactions, Occurrences and Uses, second ed., Wiley-VCH, Weinheim, 2003.
[22] F.V. Chukhrov, B.B. Zvyagin, A.I. Gorshkov, L.P. Yermilova, V.V. Korovushkin, Y.S. Rudnitskaya, N.Y. Yakubovskaya, Transl. Int. Geol. Rev. 19 (1976) 873–890.
[23] F. Haber, J. Weiss, Proc. R. Soc. Lond. A147 (1934) 332–351.
[24] D.Q.L. Oliveira, M. Goncalves, L.C.A. Oliveira, L.R.G. Guilherme, J. Hazard. Mater. 151 (2008) 280–284.
[25] L.C.A. Oliveira, T.C. Ramalho, E.F. Souza, M. Gonçalves, D.Q.L. Oliveira, M.C. Pereira, J.D. Fabris, Appl. Catal. B-Environ. 83 (2008) 169–176.
[26] J.R. Harbour, V. Chow, J.R. Bolton, Can. J. Chem. 52 (1974) 3549.
[27] S.S. Lin, M.D. Gurol, Environ. Sci. Technol. 32 (1998) 1417–1423.